Alkali interactions with a calcium manganite oxygen carrier used in chemical looping combustion

Fuel Processing Technology xxx (xxxx) xxx

Contents lists available at ScienceDirect

Fuel Processing Technology

journal homepage: www.elsevier.com/locate/fuproc

Research article

Alkali interactions with a calcium manganite oxygen carrier used in chemical looping combustion

Viktor Andersson [a], Amir H. Soleimanisalim [b], Xiangrui Kong [a], Henrik Leion [c], Tobias Mattisson [b], Jan B.C. Pettersson [a,*]

[a] Department of Chemistry and Molecular Biology, University of Gothenburg, Sweden
[b] Department of Space, Earth and Environment, Chalmers University of Technology, Sweden
[c] Chemistry and Chemical Engineering, Chalmers University of Technology, Sweden

ARTICLE INFO

Keywords:
Oxygen carrier
Chemical looping combustion
Alkali
Surface ionization detector

ABSTRACT

Chemical-Looping Combustion (CLC) of biofuels is a promising technology for cost-efficient CO_2 separation and can lead to negative CO_2 emissions when combined with carbon capture and storage. A potential challenge in developing CLC technology is the effects of alkali metal-containing compounds released during fuel conversion. This study investigates the interactions between alkali and an oxygen carrier (OC), $CaMn_{0.775}Ti_{0.125}Mg_{0.1}O_{3-\delta}$, to better understand the fate of alkali in CLC. A laboratory-scale fluidized bed reactor is operated at 800–900 °C in oxidizing, reducing and inert atmospheres to mimic CLC conditions. Alkali is fed to the reactor as aerosol KCl particles, and alkali in the exhaust is measured online with a surface ionization detector. The alkali concentration changes with gas environment, temperature, and alkali loading, and the concentration profile has excellent reproducibility over repeated redox cycles. Alkali-OC interactions are dominated by alkali uptake under most conditions, except for a release during OC reduction. Uptake is significant during stable reducing conditions, and is limited under oxidizing conditions. The total uptake during a redox cycle is favored by a high alkali loading, while the influence of temperature is weak. The implications for the understanding of alkali behavior in CLC and further development are discussed.

1. Introduction

Global warming is increasing as humans continue to add heat-trapping greenhouse gases (GHGs) to the atmosphere. Anthropogenic emissions of CO_2 have a significant contribution in GHGs emissions that often originates from fossil fuel combustion for heat and power generation [1]. One way of reducing GHGs emissions is the implementation of Carbon Capture and Storage (CCS) systems, which capture the CO_2 at the emission source and store it geologically [2]. In addition, if biomass is used as a fuel and combined with CCS technology, it would result in negative carbon dioxide emissions [3].

The technology of chemical-looping combustion (CLC) is based on unmixed combustion, and it has the same net energy release as conventional combustion. This is achieved by the use of two separate, interconnected, air and fuel reactors, which are commonly realized as circulating fluidized bed reactors [4,5]. The oxygen demand in the fuel reactor is provided by a solid oxygen carrier (OC) in the form of metal oxide particles, in contrast to conventional combustion where the oxygen demand is provided by mixing the fuel with air. The OC particles (Me_xO_y) are reduced in the fuel reactor as they release oxygen that reacts with the fuel (C_nH_{2m}), forming carbon dioxide and water as main flue gases (Eq. (1)). The reduced OC is transported to the air reactor, where it is regenerated by a chemical reaction with oxygen (Eq. (2)).

$$C_nH_{2m} + (2n+m)Me_xO_y \rightarrow nCO_2 + mH_2O + (2n+m)Me_xO_{y-1} \quad (1)$$

$$O_2 + 2Me_xO_{y-1} \rightleftarrows 2Me_xO_y \quad (2)$$

The regenerated OC is transferred back to the fuel reactor to complete the redox cycle. The circulation between the reactors is driven by loop-seals, which are often fluidized with nitrogen gas. The total heat evolving, from the endothermic reaction 1 and exothermic reaction 2, is the same as conventional combustion [4]. This way, direct contact between air and fuel is avoided, and CO_2 and water are the main product gases. Thus, a concentrated stream of CO_2 is acquired after removing the water by condensation [4]. The lack of nitrogen in the flue gas gives CLC a major advantage compared to other techniques and CO_2 sequestration

* Corresponding author.
E-mail address: janp@chem.gu.se (J.B.C. Pettersson).

https://doi.org/10.1016/j.fuproc.2021.107099
Received 2 October 2021; Received in revised form 7 November 2021; Accepted 12 November 2021

can be obtained without the need for a costly gas separation step.

To oxidize solid fuels by the OC they must first be gasified to fulfill the gas-solid reactions. Gasification of char from solid fuels is usually carried out with steam or carbon dioxide, but the process has a low reaction rate [6]. An alternative route would be if the oxygen carrier could release gaseous oxygen in the fuel reactor,

$$2Me_xO_y \rightleftarrows O_2 + 2Me_xO_{y-1} \quad (3)$$

which would result in a higher rate due to the direct reaction between gas-phase oxygen and the solid fuel [6,7]. The concept is known as chemical-looping with oxygen uncoupling (CLOU). In addition to an increased reaction rate for solid fuels, the presence of gaseous oxygen could also be advantageous by increasing the conversion of gaseous fuels [6]. The CLOU property is only possible for some OC materials, and it is based on their specific thermodynamic properties.

One of the major challenges in the CLC process is to find a viable OC with good chemical- and mechanical stability over a long period of time. Since the lifetime of the OC is expected to be lowered by solid fuels with high ash content, the interest in cheap materials as an oxygen carrier has increased in recent years. The focus has mainly been on natural ores, such as manganese ores [8,9], iron ores [10] and ilmenite [11,12]. The downside is that these materials usually have lower reactivity compared to synthetic oxygen carriers. Synthetic materials can be manufactured in a large variety of ways [13], where freeze granulation or spray-drying is often used. The most common synthetic materials are monometallic or combined oxides [14,15]. In this study, we use a manufactured calcium manganite material with CLOU properties that have been used in previous CLC studies [16,17]. The material has been proven successful by reaching high fuel conversion [18], and a long lifetime [19]. The calcium manganite can be manufactured from low cost materials, like limestone and manganese ore, and do not impose hazardous issues associated with nickel oxide materials that were previously considered to be a state-of-the-art OC [17].

Biofuels contain high levels of alkali metal compounds, with typical concentrations between 1 and 11 g kg^{-1} depending on the fuel [17]. The alkali is readily released during the heating process in a conversion system. Studies show that alkali (K and Na) may have catalytic effects on char gasification [20]. The high alkali content in biofuels is expected to increase the char conversion compared to fossil fuels [21,22]. Despite that, alkali is known to have mostly negative effects on fuel conversion applications. Silica sand is often used as bed material in conventional fluidized bed systems for combustion or gasification of biofuels. When alkali reacts with silica sand it may form viscous melts that bind the bed particles together. Over time, this often leads to bed agglomeration and defluidization [23,24]. Although silica sand is not used in CLC applications, some OC materials have a high silica content that may react with the alkali to cause similar issues [25]. Further, in some cases it could be motivated to mix OC particles and silica sand, which is done in commercial CFB units using oxygen carriers [26]. Alkali-OC interactions may occur in systems that are silica-free as well. A well-known example is the interaction between potassium and ilmenite ($FeTiO_3$) particles. Studies show that ilmenite works as an alkali scavenger by adsorbing potassium, reducing agglomeration tendencies [11,27] and lowering the alkali concentration in the product gas [28]. The proposed reason is that potassium reacts with titanium to form potassium titanate [11] which migrate to the center of the ilmenite particles over time [12]. To the best of the authors knowledge, no detailed studies of alkali interactions with calcium manganite OC material have been reported. There have been studies where this type of OC has been used for solid biomass conversion in CLC processes, but the detailed alkali-OC interactions were not investigated [17,29]. Although the operating parameters and reactor design might influence the fate of alkali in a CLC process, a fraction of the alkali end up in the flue gas stream. Alkali is released in the conversion process during the devolatilization of the fuel with subsequent char burnout, and depending on the fuel composition, KCl(g) may be a dominant species [17,30]. The volatile alkali components are carried by the flue gas to the heat extraction equipment, where the alkali may either condensate on cold surfaces or nucleate to form aerosols which can impact and deposit on the surfaces [17,24]. Therefore, alkali-induced fouling and corrosion of heat exchanger surfaces need to be considered in CLC systems [24].

Detailed studies of the behavior of alkali compounds in CLC and other thermal conversion systems are in general challenging. Industrial- or pilot-scale studies often rely on extractive sampling where condensation on existing surfaces or chemical transformations may affect the results. Studies in laboratory-scale reactors also require that wall effects are carefully considered when interpreting the results. The wall temperatures are often high due to external heating, and the surface-to-volume ratio is in general larger than in large scale facilities. In our previous study, we characterized the interactions between alkali and the inner walls of a laboratory-scale stainless steel reactor at temperatures up to 900 °C [31]. In the experiments, alkali-containing aerosol particles were fed to the reactor and alkali measurements with high time resolution were performed with a surface ionization detector (SID). It was concluded that the aerosol KCl particles vaporize when the temperature exceeds 500 °C resulting in molecular KCl that diffused quickly to the inner walls of the laboratory reactor. A fraction of the alkali reaching the walls at temperatures above 700 °C was seen to re-evaporate and leave the reactor system, whereas the alkali largely remained absorbed when reaching the walls at lower temperatures. The repeated redox cycles with alternating reducing and oxidizing atmospheres change the chemical properties of the outermost surface of the wall, which causes transient changes in the alkali concentration. The study concluded that the interactions between alkali and reactor walls need to be considered during alkali studies in laboratory setups, and the study forms the basis for the present investigations.

In the present study, a reactor on laboratory-scale designed for simulating CLC studies, is used to characterize alkali interactions with a calcium manganite perovskite OC ($CaMn_{0.775}Ti_{0.125}Mg_{0.1}O_{3-\delta}$) that has been successfully used in earlier CLC studies [16–19]. The aim is to retrieve information about the sorption kinetics and mechanisms in order to obtain a better understanding of the fate of alkali in CLC, and thereby contribute to the further development of the CLC technology. In the experiments, alkali is fed to the system as aerosol KCl particles, while alkali- and gas concentrations in the exhaust are measured online. Potassium chloride was selected for this study since potassium is a major alkali component in biofuels and KCl(g) is readily formed when Cl is available [17,24,32]. Recurring inert, reducing and oxidizing atmospheres at temperatures between 800 and 900 °C are used to investigate how the OC interact with alkali. Alkali uptake on the OC is observed to dominate under the investigated conditions with significant effects of gas composition and alkali loading, and the implications for CLC processes and further laboratory studies are discussed.

2. Experimental

A schematic of the laboratory-scale reactor used to investigate the interactions between alkali and OC is shown in Fig. 1, and a more detailed description has been presented elsewhere [31]. Other studies on laboratory scale have been using similar types of reactors [33,34]. The fluidized bed reactor is 915 mm long with an inner diameter of 26 mm and it is operated with external heating. The reactor wall material is alloy 304 stainless steel and the gas distributor plate and particle filter inside the reactor is alloy 316. Constant operation temperatures of 800, 850 and 900 °C are used in the study.

The reactor has been used for approximately half a year with regular redox studies before the present experiments. Therefore, a thin oxide scale is expected to have formed on the wall surface prior to the experiments presented in this work. Severe corrosion of the reactor walls is neither expected nor observed and the alkali loadings used in earlier studies are similar to those used here. Sporadic disassembling and

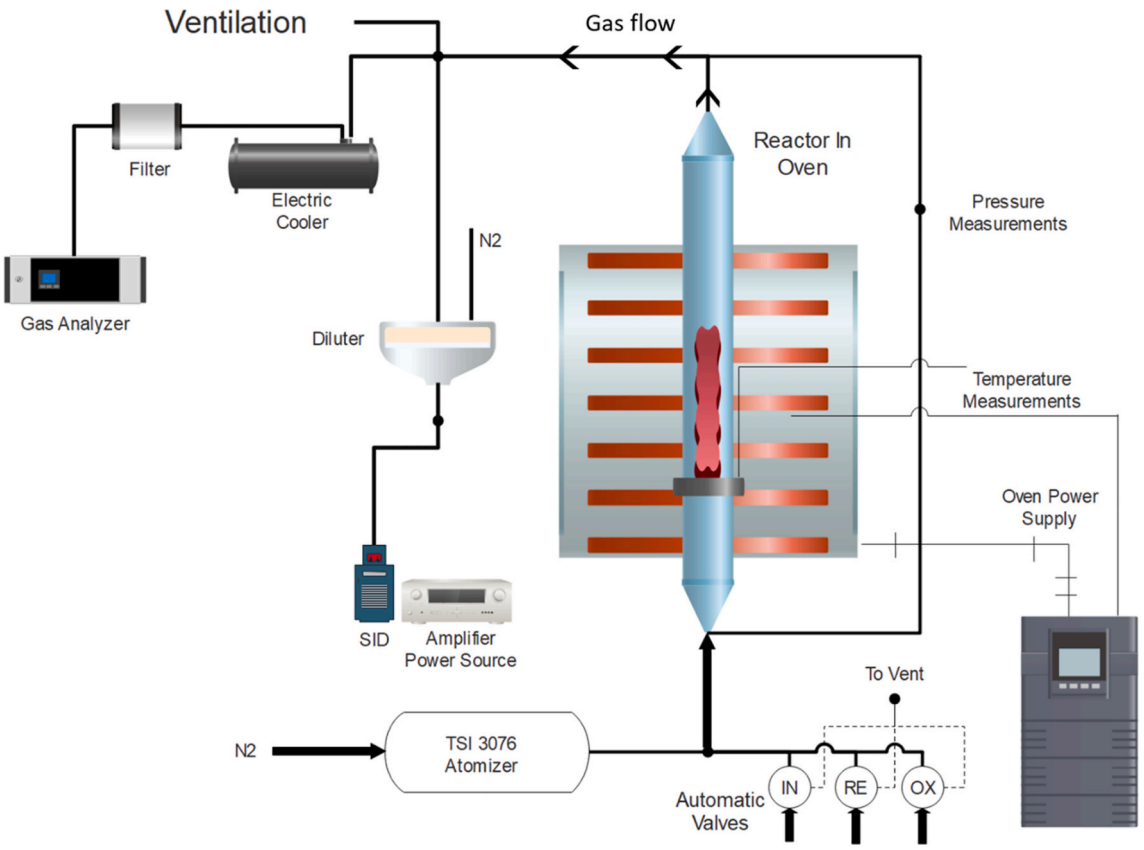

Fig. 1. Schematic of the externally heated laboratory-scale reactor with automatic gas-feeding system and an atomizer (alkali aerosol generator). Fractions of the exhaust gases leaving the reactor are fed to a gas analyzer and an alkali measurement system SID.

cleaning with soap and water have been done without influencing the observations in the study.

Sub-micron alkali salt particles are introduced to the fluidized bed system [21,35]. The particles were continuously generated from a KCl water solution by using an aerosol particle generator (Model 3076, TSI Inc.). A flow of pure nitrogen atomized the KCl solution, and subsequently dried in an open path diffusion dryer to produce dry (20% relative humidity) KCl aerosol particles at room temperature [36]. The KCl particles had a size distribution with an average diameter of 45 to 57 nm, which was established by adjusting the concentration of KCl in the solution. The alkali particles, suspended in 2 L min^{-1} flow of nitrogen, were led to the reactor by a conductive tube. Aerosol losses to the 1.5 m long and 8 mm wide tube walls can be neglected in the particle size range used in this study [37]. The flow of alkali particles was mixed with the reactor gases before being fed to the fluidized bed reactor.

Two different KCl concentrations of 5 or 10 mM were used in the water solution, resulting in 6 or 12 mg KCl m^{-3} inlet gases, henceforth denoted as medium and high alkali loading. The used loadings are within range of typical alkali concentrations measured during biofuel combustion in CLC (1–35 mg m^{-3}) [17].

Different inlet gases were fed to the reactor system at a constant total gas flow to mimic the reducing, oxidizing and inert conditions present in the different parts of a CLC system during biomass combustion. The reducing and oxidizing atmospheres were obtained by using a mixture of 50% H_2 in CO and 21% O_2 in N_2, respectively. The inert atmosphere was simulated using pure nitrogen. The flow entering the reactor system consisted of 2 L min^{-1} nitrogen containing alkali particles from the aerosol generator, mixed with 0.3 L min^{-1} of the reducing, oxidizing or inert gases. The result was a 2.3 L min^{-1} gas mixture of KCl aerosol particles in either pure nitrogen, 6.5 vol% CO and 6.5 vol% H_2 in nitrogen or 2.7 vol% O_2 in nitrogen. Each reactor experiment consisted of several redox cycles in series, with each cycle composed of: 180 s inert, 1000 s reducing, 500 s inert and lastly, 1450 s oxidizing atmospheres.

The exhaust gases leaving the reactor were separated into three streams. The first flows through a diluter (diluting the sample gas by a factor of 10 with nitrogen) to a surface ionization detector (SID), which conducts measurements of alkali concentration online. The SID instrument has been thoroughly described in previous studies [22,28,38]. It uses the technique of surface ionization to measure the total concentration of K and Na with high time resolution, and it has been used in various studies focusing on gasification and combustion [17,22,28,38]. The second stream leaving the reactor flows through a particle filter and a cooler to a gas analyzer (Model NGA 2000, Emerson Electric Co.) which measures the O_2, CO_2, CO, CH_4 and H2 concentrations in the gas. Lastly, the third flow leaving the reactor is led to ventilation.

Experiments were carried out both with an empty reactor to characterize the interactions between alkali and the reactor walls, and with the reactor filled with a bed of 20 g of OC that was fluidized by the inlet gas flow. The OC consisted of calcium manganite with additions of titanium oxide and magnesium oxide. The OC molar composition is $CaMn_{0.775}Ti_{0.125}Mg_{0.1}O_{3-\delta}$. It was prepared by The Flemish Institute for Technological Research, Belgium, (VITO) in 2013 and was manufactured by spray-drying. The OC has a perovskite structure where Ca, Mn, Ti and O bind together and the Mg occurs in a separate phase [39]. The oxygen deficiency in the perovskite structure is defined by the δ-factor, which is a function of the surrounding oxygen fugacity, meaning that δ is large in a CLC fuel reactor and small in an air reactor [40]. The particles have a poured bulk density of 1300 kg/m^3 and a size range of 90–250 μm. The particles have been used previously in 10 kW pilot experiments with gaseous fuels and are considered not to contain any significant ash components (*e.g.* alkali) [39]. However, as described in the Results section, the material contains a low concentration of ilmenite particles from previous use.

Samples of oxygen carrier material before and after use in the reactor

were molded in epoxy and the surface was polished to enable cross-section analysis of particles. The samples were analyzed with a scanning electron microscope (SEM) and the elemental composition was determined with energy-dispersive x-ray spectroscopy (EDX).

3. Results

The main experimental results consist of alkali and gas concentrations measured under different conditions with respect to temperature (800, 850 or 900 °C), alkali loading (no alkali, medium loading (6 mg m^{-3}), or high loading (12 mg m^{-3})), and with or without an OC fluidized bed in the reactor. The reactor was operated with a constant gas flow of 2.3 L min^{-1} with recurring reducing, oxidizing and inert atmospheric conditions to complete the redox cycles described above. The introduced KCl aerosol rapidly evaporates at temperatures higher than 500 °C, and the discussed experiments consequently concern KCl in molecular form within the reactor [31]. The temperature decreases, causing alkali aerosol particles to be formed again by nucleation, downstream of the heated reactor section [31]. The main results are presented in the following three sub-sections and complementary analyses of bed material are presented in Section 3.4.

3.1. Alkali concentrations during repeated redox cycles

Typical results from experiments with and without bed material in the reactor are shown in Fig. 2. The experiments were performed with 6 mg KCl m^{-3} (medium alkali loading) during several consecutive redox cycles and with an operating temperature of 900 °C. Although gas and alkali concentrations change within each redox cycle, high reproducibility is observed between the cycles. The same can be said about the reproducibility between experiments on different days when using the same operating conditions. The results obtained without bed material in the reactor are characterized by a general loss of alkali compared to the inlet alkali concentration. Changes in gas concentration lead to large transient changes in alkali concentration, in agreement with earlier studies [31]. The results obtained with a fluidized bed of OC-particles in the reactor follow a distinctly different pattern with minor variation between the different stages compared to the observations for an empty reactor.

Single redox cycles in Fig. 2 are illustrated in greater detail in Fig. 3. The panels contain colored areas indicating oxidizing (blue), inert (white) and reducing (orange) atmospheres. KCl interacts strongly with the inner steel surface of the empty reactor (Fig. 3a). Transient behavior is observed when changing gas composition and the alkali concentration typically relaxes to new conditions in a few hundred seconds. Distinct transient changes are observed when reducing conditions are turned on and off, while the transient effects are substantially smaller when switching between inert and oxidizing atmospheres. The observed

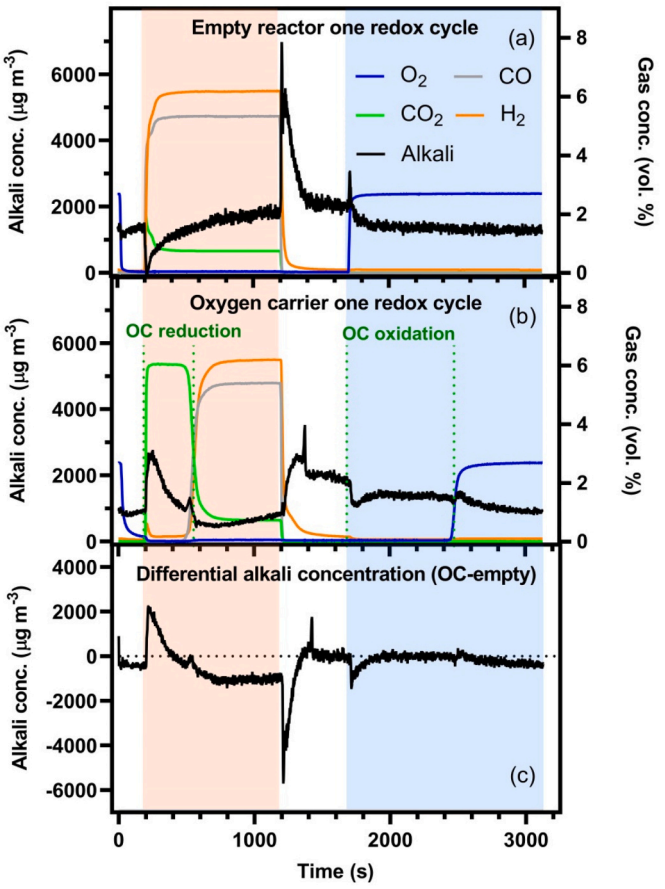

Fig. 3. Measurements of outlet alkali- and gas concentrations conducted during one redox cycle in (a) empty reactor and (b) oxygen carrier experiments with an alkali loading of 6 mg m^{-3} and 900 °C reactor temperature. Colored areas mark stages with oxidizing (blue), inert (white) and reducing (orange) atmospheres. Dotted lines in (b) marks time periods when the OC undergoes reduction and oxidation. (c) The differential alkali concentration obtained by subtracting the concentration measured without OC in the reactor (a) from the results obtained with OC in the reactor (b). (For interpretation of the references to colour in this figure legend, the reader is referred to the web version of this article.)

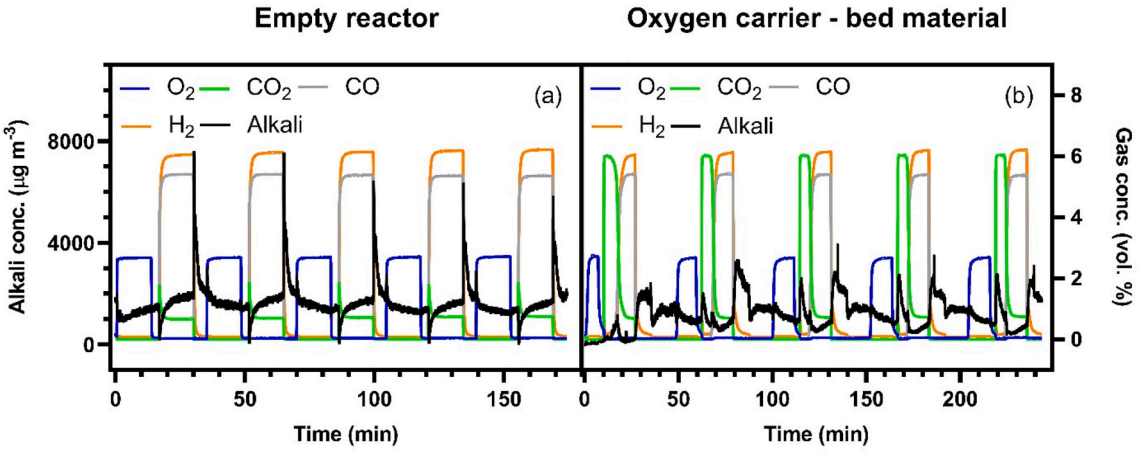

Fig. 2. Gas and alkali concentrations measured in the outlet from (a) an empty reactor, and (b) a reactor containing an OC fluidized bed. The alkali loading was 6 mg m^{-3} and the reactor temperature was 900 °C. Figures illustrate five consecutive redox cycles.

changes have previously been related to chemical changes in the composition of the outermost layer on the stainless steel [31].

The alkali behavior is markedly different with an OC fluidized bed present in the reactor (Fig. 3b). Changes in gas composition lead to changes in the alkali level. Still, the transient behavior is generally less pronounced and observed patterns in the alkali level are not always in the same direction as the observed patterns with an empty reactor. The most notable example is an increase in alkali concentration at the beginning of the reducing phase when an OC bed is present compared to the observed behavior with an empty reactor. In addition, changes in alkali level are observed due to oxidation and reduction of the OC. When oxidizing conditions are applied, the observed oxygen level is initially low due to reaction with the OC, and the oxygen level increases after approximately 700 s when the process is completed. The completion of the OC oxidation process is associated with a decrease in alkali signal. In a similar way, reduction of the OC initially results in the formation of CO_2 (and H_2O), and the reducing gases (CO and H_2) appear after about 400 s when the reduction of the bed is completed. And again, the alkali concentration changes in connection with changes in OC properties.

Fig. 4 summarizes the resulting alkali concentrations from experiments when the reactor was operated at 800, 850 and 900 °C using three different alkali loadings. The results for an empty reactor are shown in Fig. 4a-c, and the results while using an OC fluidized bed in Fig. 4d-f.

A small release of alkali from the reactor wall is observed in empty reactor experiments where no alkali is injected into the system (Fig. 4a). Switching gas composition results in slight increase in intensity, and the effect is most pronounced when turning to an inert atmosphere from a reducing atmosphere. The corresponding results using medium alkali loading (Fig. 4b) show a characteristic pattern with minor differences with regard to temperature. In general, the trends seen for a high loading confirm those with medium loading (Fig. 4c), but with a more pronounced temperature dependence during the inert stage following the reducing stage.

The corresponding results for a reactor containing a fluidized bed are displayed in Fig. 4d-f. In experiments without alkali injection (Fig. 4d), the alkali concentration is initially low during the reducing period before increasing to a higher level. In oxidizing atmosphere, the alkali signal is low when the OC undergoes oxidation, and higher after oxidation is completed. Comparison with the results for an empty reactor (Fig. 4a) suggests that the OC is taking up alkali released from the reactor wall while the material undergoes both reduction and oxidation.

The OC-results with medium alkali loading are depicted in Fig. 4e. The introduction of reducing gases initially results in a major increase in alkali concentration compared to the empty reactor case, and the observed concentration shows a distinct temperature dependence. The alkali signal is low when the OC is fully reduced. In the oxidizing atmosphere, the alkali signal is initially higher during the oxidation process and lower when the OC is fully oxidized.

Large uptake of alkali is observed in high alkali loading experiments with OC present (Fig. 4f). This is evident as the measured alkali concentrations are in general comparable to medium alkali loading, while

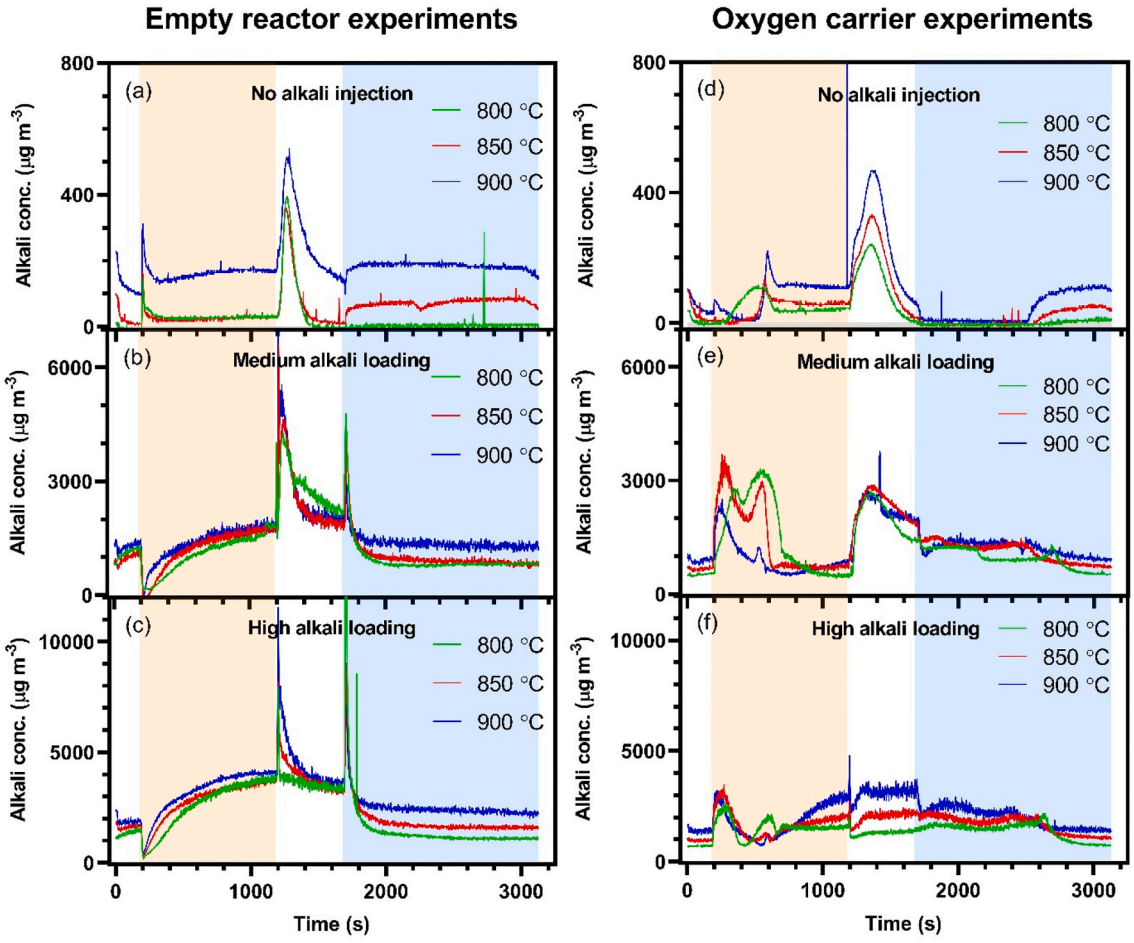

Fig. 4. Alkali concentrations measured during experiments in (a-c) empty reactor and (d-f) with oxygen carriers present. Colored areas mark stages with oxidizing (blue), inert (white) and reducing (orange) atmospheres. Different panels show results obtained with different inlet concentrations of KCl: (a, d) no alkali injection, (b, e) medium alkali loading (6 mg m^{-3}), and (c, f) high alkali loading (12 mg m^{-3}). Results obtained when the reactor operates at temperatures of 800, 850 and 900 °C are displayed. (For interpretation of the references to colour in this figure legend, the reader is referred to the web version of this article.)

the inlet concentration is doubled. In reducing atmosphere, alkali peaks are observed as the OC is being reduced. When the OC has been fully reduced and conversion stops, the OC seems to adsorb large amounts of the alkali at a steady rate at 800 °C, whereas the alkali signal gradually increases with time at 900 °C.

3.2. Alkali uptake and release from the oxygen carrier

We next evaluate the uptake and release of alkali from the OC during different stages of the redox cycle in further detail. The analysis is based on a comparison between the alkali concentrations measured with and without OC bed material in the reactor. A measured alkali concentration that is lower than obtained with an empty reactor is interpreted as alkali uptake by the OC, while a higher concentration is interpreted as alkali release from the OC.

As described above, Figs. 2–4 display alkali concentrations and Figs. 2 and 3 include gas concentrations with and without OC-particles in the reactor. Fig. 3c shows the differential alkali concentration obtained by subtracting the concentration measured without OC in the reactor (Fig. 3a) from the results obtained with OC in the reactor (Fig. 3b). The observed difference is negative or close to zero for most conditions. The initial part of the reducing stage, with positive values, is an exception suggesting alkali release from the OC. Qualitatively similar results are obtained for other investigated cases (see Supplemental Information, Fig. S1).

The alkali release and uptake for different stages during the redox cycle are presented in Fig. 5. The reducing and oxidizing stages are each separated into two parts corresponding to before and after completion of the oxidation or reduction processes, as revealed by changes in gas concentrations (see Fig. 3b). The displayed data are produced by integrating the total alkali signal during each of the six stages in experiments with a fluidized bed, and removing the integrated signals from experiments with an empty reactor during the corresponding time periods,

$$OC_{alkali,i} = \int OC_i - \int Empty\ reactor_i \quad (4)$$

where i = *inert 1, red 1, red 2, inert 2, ox 1* and *ox 2,* and the OC release alkali if $OC_{alkali} > 0$ and absorb alkali if $OC_{alkali} < 0$. The transition points in the reducing and oxidizing stages are set when 50% of the final gas concentration has been reached. Thus, the transition between *red 1* and *red 2* occurs when $[H_2] = [H_{2,\ final}]/2$ and the transition between *ox 1* and *ox 2* occurs at the time when $[O_2] = [O_{2,\ final}]/2$.

The integrated alkali uptake over a complete redox cycle is marked SUM in Fig. 5. The uptake is close to zero for a medium alkali loading and temperatures of 800 and 850 °C, but becomes substantial at 900 °C. In contrast, the total alkali uptake is substantial at all temperatures for high loading. Most individual stages are characterized by either alkali uptake or a minor influence of the OC. The only exception with pronounced alkali release from the OC occurs during the initial part of the reducing stage when using medium alkali loading. The inert stages show similar levels as the preceding stages, indicating that OC properties remain primarily unchanged when switching to inert conditions. Uptake is in general considerably more pronounced during reducing conditions compared to oxidizing conditions, which is particularly clear when using a high alkali loading. There is a small overall tendency to increase uptake with increasing temperature, but the effect is small and individual stages show different trends with increasing temperature.

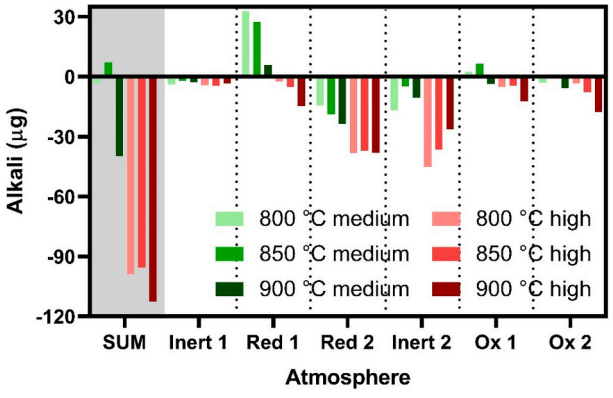

Fig. 5. Net alkali uptake and release from the oxygen carrier. The values correspond to the integrated alkali signal from a fluidized bed minus the integrated alkali signal from an empty reactor during the corresponding time period (see text for details). Negative values mean net alkali uptake by the OC and positive values mean net alkali release from the OC. Colored bars mark the alkali loading with medium (green) and high (red) loading at temperatures of 800, 850 and 900 °C. The grey field marks the total amount of adsorbed/released alkali over a complete redox cycle. (For interpretation of the references to colour in this figure legend, the reader is referred to the web version of this article.)

3.3. Time dependent alkali uptake and release

The transient signals caused by the alkali-wall interactions mostly obscure the temporal variation of alkali-OC interactions, but some interesting observations are summarized here. Fig. 6 compares the alkali concentrations measured with and without an OC bed in the reactor at 800 °C. No alkali is injected into the system in this case, and the emitted alkali thus originates from either the wall or the OC bed material. Note that the type of alkali compound involved is not identified, and the case may not be entirely comparable to the KCl loading cases. The observed signal is likely to be due to a potassium-containing compound since potassium has been used extensively in the reactor. It is less clear if KCl is the dominant species, and KOH formed by reaction with H_2O is a likely alternative.

First, a short intense alkali release is observed when switching from the reducing to the inert atmosphere in the empty reactor (Fig. 6a). The

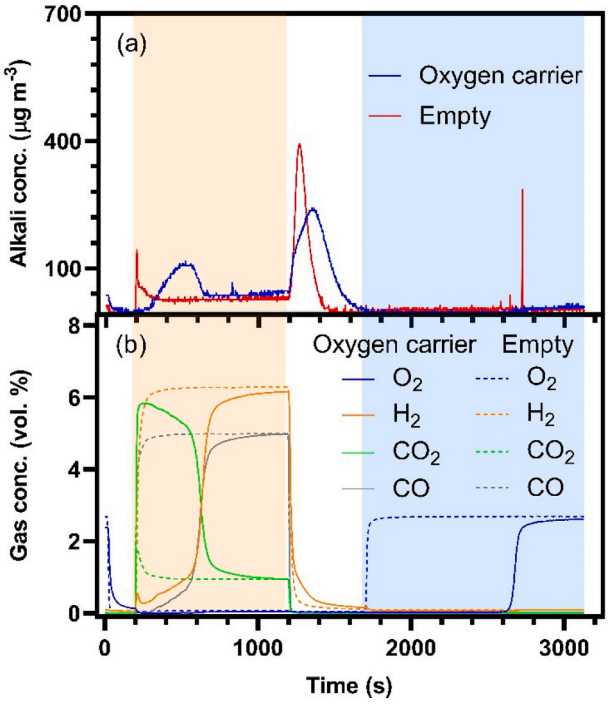

Fig. 6. (a) Alkali concentrations and (b) gas concentrations measured during empty reactor and oxygen carrier experiments with no alkali injection at 800 °C. Colored areas mark stages with oxidizing (blue), inert (white) and reducing (orange) atmospheres. (For interpretation of the references to colour in this figure legend, the reader is referred to the web version of this article.)

same alkali release from the reactor wall is expected to happen when a bed is present, and the transient signal may be considered as a sharp peak in alkali flux reaching the fluidized bed. This is thus the equivalent of a pulse experiment. The corresponding peak, while the reactor is filled with the OC bed, is broader and delayed compared to the flux reaching the bed. The total peak areas are similar and we conclude that most of the released alkali is able to escape from the bed, but transport processes and interactions with the fluidized bed affect the time dependence of the peak. The initial part of the peak observed with OC present displays a rapid increase in intensity, similar to the initial increase in signal when using an empty reactor. This suggests that a portion of the flow exits the fluidized bed quicker than the majority, *i.e.* part of the flow is able to short-circuit the fluidized bed and pass through with minimal retention.

Second, a broad peak is observed in Fig. 6a during the reducing phase when an OC fluidized bed is present. The changes in alkali concentration for an empty reactor during the same period are small, and the observed peak can safely be concluded to be due to alkali emission from the OC.

Furthermore, the gas analysis from the OC experiment indicates that different concentrations of CO and H_2 are detected after 800 s, *i.e.* after the OC has been fully reduced. The fuel gas contains 50% H_2 in CO and the outlet concentrations of CO and H_2 should therefore be equal. However, based on the empty reactor experiments (marked with dotted lines in Fig. 6b), a fraction of the CO is converted to CO_2 with the sum of CO and CO_2 equal to that of H_2. Therefore, the conversion of CO to CO_2 after 800 s in the OC experiments likely originates from processes related to the reactor walls and not the OC material, and the effect is therefore not further explored in the present study.

3.4. Characterization of oxygen carrier materials

We have carried out complementary studies where the bed material has been characterized with SEM and EDX before and after use in the reactor experiments. The used samples were exposed to five consecutive redox cycles with medium or high alkali loading.

The OC material used in this study is calcium manganite with additions of titanium and magnesium oxide ($CaMn_{0.775}Ti_{0.125}Mg_{0.1}O_{3-\delta}$). The cross sectional SEM analysis of a calcined OC sample not used in the reactor experiments (Fig. 7) shows that spherical particles dominate in the sample. The colour maps (Fig. 7b-e) show that the spherical particles contain Ca, Mn and Ti bound together in the structure, while Mg occurs in a separate phase. The colour map shows that all particles also contain small amounts of potassium (Fig. 7g).

In addition, the elemental mapping also visualize two non-spherical particles made of Fe and Ti with a Ca-rich outer layer (Fig. 7b, d and f). These particles are ilmenite ($FeTiO_3$) [11]; therefore, the analysis confirms the presence of ilmenite in the sample received from previous experiments of the OC material in a different reactor [39].

Analysis of OC samples that have been used in the lab-reactor at

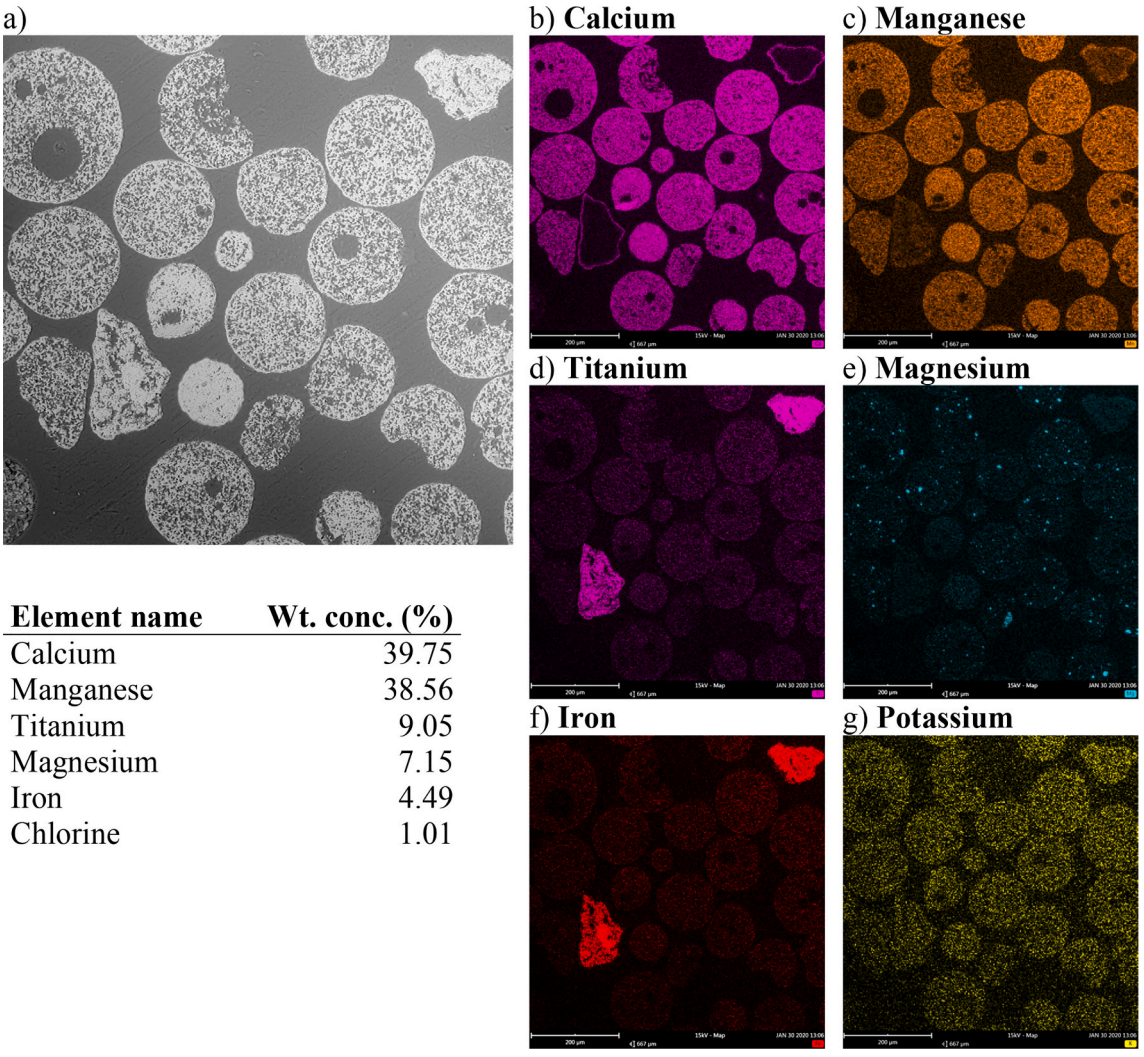

Element name	Wt. conc. (%)
Calcium	39.75
Manganese	38.56
Titanium	9.05
Magnesium	7.15
Iron	4.49
Chlorine	1.01

Fig. 7. (a) SEM overview of the cross section of unused OC, (b-g) colour map of the elemental composition, FOV = 667 µm, 15 kV – Map. Table 1: Elemental composition of unused OC.

900 °C with medium and high alkali loadings are shown in Figs. S2 and S3 and Tables S1 and S2 in Supplemental Information. No significant changes in composition or morphology are observed from the SEM-EDX analyses before and after use in the reactor experiments.

It has been seen in previous studies that potassium is adsorbed by ilmenite particles [11,12], where a reaction between potassium and titanium is suggested to form potassium titanate. The present analysis indicates that the potassium concentrations are low and comparable in both ilmenite and calcium manganite particles.

4. Discussion

4.1. Methodology for laboratory-scale studies of alkali-OC interactions

Before focusing on the details regarding the interactions between alkali and OC, we begin by addressing challenges in studying alkali processes on the laboratory-scale. Alkali-containing compounds will interact relatively strongly with hot surfaces in their vicinity as illustrated by the present study and previous work [31]. This includes reactor walls, oxygen carriers, fluidized bed particles and gas extraction probes.

The reactor employed here is a typical setup for fluidized bed studies on laboratory-scale. Alkali is injected into the system in a controlled way, but the properties of the reactor walls influence the actual amount of alkali that is able to reach and interact with the OC bed particles. Detailed interactions between oxygen carriers and alkali may therefore be obscured by the large effects from the reactor wall. However, excellent reproducibility is seen between different experiments when experimental conditions are maintained. This helps separate the effects of the reactor walls from oxygen carrier interactions on the observed alkali concentrations. It is, therefore, possible to obtain highly valuable information about the overall process even though it is difficult to separate the effects from different factors.

Changing the geometry and reactor material may potentially reduce the effects of wall interactions. Another reactor material with higher corrosion resistance and different properties under atmospheres with varying oxygen activities and reduction potentials may outperform the 304 alloy used in this study. Although high temperature characteristics are relatively well known for alloy 304 under oxidizing conditions, surface properties and reactions with alkali in reducing conditions are less well studied [31]. Other potential materials share the same problems, and separate studies of the interaction between alkali and materials in both reducing and oxidizing conditions are likely required to find the optimal material.

Another way of reducing the alkali-wall interactions is to limit the area of hot walls. Although it might be impossible to completely avoid interactions, changing the geometry of the reactor may still be beneficial. Steep temperature gradients are of particular interest as it allows the alkali to be in the form of aerosol particles below certain temperatures and thus limit the amount of gaseous alkali reaching the wall. The low diffusion coefficients of aerosol particles compared to alkali compounds in molecular form significantly reduces their ability to reach any surfaces in the experimental system [31]. In addition, it is favorable if the total surface area of the fluidized bed particles is much larger than that of adjacent walls. It is argued that several of these factors should be carefully considered in order to strengthen our ability to characterize alkali processes in laboratory-scale experiments.

4.2. Alkali interactions with the oxygen carrier

To interpret the experimental results, the properties of the OC under different applied conditions need to be considered. The OC used in the present study has a molar composition of $CaMn_{0.775}Ti_{0.125}Mg_{0.1}O_{3-\delta}$, where the oxygen deficiency (δ) is large during reducing conditions and small in oxidizing conditions [40]. The perovskite structure of the OC material can be written as $ABC_{3-\delta}$, where A and B are large and small cations and C is oxygen. The addition of Ti in the B-site of the lattice structure stabilizes the perovskite and keeps the structure intact at low partial pressures of oxygen [41]. The magnesium is not part of the calcium manganite structure (see Fig. 7), and does not increase the chemical stability of the OC.

The OC material is known to release gaseous oxygen under suitable conditions. This is confirmed by the present results (*e.g.* Fig. 3b) where the oxidized OC releases 0.2 vol% (≈ 0.004 L_n/min) oxygen while the bed is fluidized with nitrogen. Rydén et al. report that a similar OC material released 0.007–0.025 L_n/min O_2 at 800–900 °C when fluidized with CO_2 [18]. The OC was oxidized with an oxygen activity of $pO_2 = 0.21$ atm in their study, while $pO_2 = 0.027$ atm is used here, and the change in O_2 partial pressure during the reoxidation has been observed to affect the oxygen release during OC reduction [18].

An earlier study by Hallberg et al. showed that 99 h of operation did not affect the ability of the OC to release oxygen to an inert atmosphere [39]. The same study showed no change in reactivity with fuel, whereas a similar study in a smaller reactor unit showed a small decrease in reactivity after 40 h of operation [42]. It was suggested that the slight change in reactivity in the smaller unit was due to inadequate circulation, which may lead to a larger reduction of the OC. In the present study, the reducing atmosphere is kept for an additional 500 s after the OC is fully reduced, which may lead to a larger degree of reduction than in a circulating CLC unit. It would thus be possible to see slight reactivity changes during an experiment, but this has not been confirmed and the redox properties and reactivity have been constant throughout the study. Studies of alkali-OC interactions are scarce and to our knowledge, no earlier investigation focussing on alkali interactions with calcium manganite has been reported. In a related study, Gogolev et al. measured alkali concentrations in a 100 kW CLC unit operated with various solid biomass fuels and a mixture of ilmenite and $CaMn_{0.775}Ti_{0.125}Mg_{0.1}O_{3-\delta}$ [17]. The inventory initially consisted of 10–20 wt% ilmenite. To make up for losses fresh ilmenite was continuously fed to the system raising the fraction to approximately 80 wt% at the end of the campaign. The alkali concentration of the OC was 0.18 wt% before and 0.47 wt% after operation indicating alkali accumulation [17]. Although ilmenite is known to adsorb alkali [11,12] the calcium manganite may also have contributed to the alkali uptake. The results are consistent with the present findings, and further investigations using the same OC mixtures in both setups would be valuable. Another related study used a similar calcium manganite for CLC of wood char in a 10 kW reactor unit, but the OC alkali content and interactions in the system were not considered [29].

In experiments with a high alkali loading around 95–112 μg of KCl is absorbed by the OC in each complete redox cycle (see Fig. 5). Assuming that all OC particles are spherical with a diameter of 150 μm, the total geometric area of the bed material is approximately 2000 cm^2 (assuming an OC density of 2000 kg m^{-3}). Using these values, the average KCl uptake is 0.2 monolayers ($2{\cdot}10^{14}$ molecules cm^{-2}), if a complete monolayer is assumed to contain $\sim 1{\cdot}10^{15}$ molecules cm^{-2}. This value should be considered as an upper limit since particles are not perfect spheres and diffusion into the OC bulk material may be substantial, and the actual surface coverage could be considerably lower. In addition, the small ilmenite fraction in the used OC material may efficiently absorb the injected alkali into the reactor [11,12]. If a significant surface coverage would indeed build up in a limited number of redox cycles, we would expect an influence on reactivity. However, no major change in OC performance was observed during the experiments. Nevertheless, uptake is substantial and future experiments during more prolonged periods would be valuable to evaluate any long-term effects on OC performance.

Chemical reactions between KCl and components in the surface layer must be responsible for the observed alkali uptake, but the identification of the actual products and structures involved will require additional studies with other methods. Changes in gas composition under reducing and oxidizing conditions affect the surface properties and thereby the

alkali binding sites. The concentrations of main gas components are monitored online during the experiments, but the measurements do not include water vapor. The amount of water entering the system from the aerosol generator is low, but significant amounts of water are formed in the fuel conversion process during the reducing stage. Water may potentially react with potassium to form potassium hydroxide, which has a relatively high vapor pressure and the process may be a contributing factor behind the observed alkali release during the fuel conversion process. In an actual CLC system, water vapor is always present as long as fuel is converted and its relevance for alkali-OC interactions needs further investigation in future work.

4.3. Implications for CLC studies

The results from the present study may be used to discuss the behavior of alkali in a CLC process consisting of two interconnected air and fuel reactors [5,6]. Alkali is a significant component in biofuels and it is consequently introduced to the fuel reactor of a CLC system together with the fuel. A fraction of the alkali is released to the gas phase during fuel conversion. According to the present study, the released alkali is likely to be absorbed by a calcium manganite OC while it is reduced in the fuel reactor. This uptake process will continue in the subsequent loop seal leading to the air reactor (if alkali remains present in the gas phase). Inside the air reactor, the alkali absorbed by the OC appears to be relatively stable and alkali release may be expected to be limited. If the air reactor contains alkali (*e.g.* if alkali is transported from the fuel reactor to the air reactor as ash particles), the OC may continue to absorb alkali during the reoxidation process. The same can be said when the OC is transported through the second loop seal, leading the particles back to the fuel reactor. Entering the fuel reactor, the oxidized OC will initially release O_2 and alkali while being reduced, and absorb alkali when fully reduced.

The studied alkali-OC interactions are dominated by alkali uptake under most studied conditions, except for some release when the OC undergoes reduction. An alkali release in the fuel reactor is likely to be beneficial due to the catalytic effects of alkali on fuel conversion processes [20]. Alkali release in the fuel reactor may also lead to relatively high alkali concentrations in the flue gases from the fuel reactor, which is prefered over release in the air reactor where high alkali concentrations may lead to corrosion and fouling of heat exchanger surfaces.

5. Conclusions

Experiments have been carried out with the aim to investigate alkali interactions with an OC ($CaMn_{0.775}Ti_{0.125}Mg_{0.1}O_{3-\delta}$) used in CLC applications. Alkali was fed continuously to the laboratory-scale fluidized bed reactor in the form of aerosol KCl particles, and experiments were performed at temperatures from 800 to 900 °C under recurring reducing, inert and oxidizing atmospheres with repeated redox cycles. The main conclusions are:

- Stable and repeatable conditions can be achieved with the present experimental setup, which helps to distinguish the influences of alkali-OC interactions from alkali interactions with the reactor wall.
- Alkali is absorbed by the OC under most studied conditions, with the exception being conditions where the OC is undergoing reduction and alkali release is observed.
- Alkali uptake is substantially larger under stable reducing conditions than under oxidizing conditions.
- Alkali uptake increases considerably with increasing gas phase alkali concentration.
- An increased temperature appears to promote alkali uptake under oxidizing conditions, while the trends are less clear and depend on experimental conditions in reducing and inert atmospheres.
- Alkali uptake and release need to be carefully considered under CLC process conditions.

Several future experiments may help to improve the understanding of alkali-OC interactions, including systematic studies of the effects of gas composition and OC properties. Investigations with other reducing gases like CH_4 combined with detailed material analyses may help to understand the uptake of alkali observed under reducing conditions. Experiments with different alkali compounds that are expected in thermal conversion systems, like KOH, are also likely to be valuable, as well as studies covering a wider temperature range than used here. In addition, improvements of the experimental methodology are currently under way to reduce the influence of wall effects and to provide information about the kinetics of alkali-OC interactions.

Declaration of Competing Interest

The authors declare no conflict of interest.

Acknowledgment

This work carried out within the “Biomass combustion chemistry with oxygen carriers” project, funded by the Swedish Research Council 2016-06023.

Appendix A. Supplementary data

Supplementary data to this article can be found online at https://doi.org/10.1016/j.fuproc.2021.107099.

References

[1] G. Myhre, D. Shindell, F.-M. Bréon, W. Collins, J. Fuglestvedt, J. Huang, D. Koch, J.-F. Lamarque, D. Lee, B. Mendoza, T. Nakajima, A. Robock, G. Stephens, T. Takemura, H. Zhang, Anthropogenic and natural radiative forcing, in: T. F. Stocker, D. Qin, G.-K. Plattner, M. Tignor, S.K. Allen, J. Boschung, A. Nauels, Y. Xia, V. Bex, P.M. Midgley (Eds.), Climate Change 2013: The Physical Science Basis. Contribution of Working Group I to the Fifth Assessment Report of the Intergovernmental Panel on Climate Change, Cambridge University Press, Cambridge, United Kingdom and New York, NY, USA, 2013.

[2] J. Alcalde, S. Flude, M. Wilkinson, G. Johnson, K. Edlmann, C.E. Bond, V. Scott, S. M.V. Gilfillan, X. Ogaya, R.S. Haszeldine, Estimating geological CO2 storage security to deliver on climate mitigation, Nat. Commun. 9 (2018) 2201.

[3] T. Mattison, F. Hildor, Y. Li, C. Linderholm, Negative emissions of carbon dioxide through chemical-looping combustion (CLC) and gasification (CLG) using oxygen carriers based on manganese and iron, Mitig. Adapt. Strateg. Glob. Chang. 25 (2020) 497–517.

[4] A. Lyngfelt, B. Leckner, T. Mattisson, A fluidized-bed combustion process with inherent CO2 separation; application of chemical-looping combustion, Chem. Eng. Sci. 56 (2001) 3101–3113.

[5] A. Lyngfelt, Oxygen Carriers for Chemical Looping Combustion - 4 000 h of Operational experience, Oil Gas Sci. Technol. 66 (2011) 2.

[6] T. Mattisson, A. Lyngfelt, H. Leion, Chemical-looping with oxygen uncoupling for combustion of solid fuels, Int. J. Greenhouse Gas Control 3 (2009) 11–19.

[7] H. Leion, T. Mattisson, A. Lyngfelt, Using chemical-looping with oxygen uncoupling (CLOU) for combustion of six different solid fuels, Energy Procedia 1 (2009) 447–453.

[8] Y. Li, Z. Li, L. Liu, N. Cai, Measuring the fast oxidation kinetics of a manganese oxygen carrier using microfluidized bed thermogravimetric analysis, Chem. Eng. J. 385 (2020), 123970.

[9] A. Pérez-Astray, T. Mendiara, L.F. de Diego, A. Abad, F. García-Labiano, M. T. Izquierdo, J. Adánez, Improving the oxygen demand in biomass CLC using manganese ores, Fuel 274 (2020), 117803.

[10] J. Adanez, A. Abad, F. Garcia-Labiano, P. Gayan, L.F. de Diego, Progress in Chemical-Looping Combustion and Reforming technologies, Prog. Energy Combust. Sci. 38 (2012) 215–282.

[11] A. Corcoran, J. Marinkovic, F. Lind, H. Thunman, P. Knutsson, M. Seemann, Ash Properties of Ilmenite used as Bed Material for Combustion of Biomass in a Circulating Fluidized Bed Boiler, Energy Fuel 28 (2014) 7672–7679.

[12] A. Corcoran, P. Knutsson, F. Lind, H. Thunman, Mechanism for migration and layer growth of biomass ash on ilmenite used for oxygen carrier aided combustion, Energy Fuel 32 (8) (2018) 8845–8856.

[13] N.M. Pour, G. Azimi, H. Leion, M. Rydén, A. Lyngfelt, Production and examination of oxygen-carrier materials based on manganese ores and ca(OH)2 in chemical looping with oxygen uncoupling, AICHE J. 60 (2014) 645–656.

[14] T. Mattisson, M. Keller, C. Linderholm, P. Moldenhauer, M. Rydén, H. Leion, A. Lyngfelt, Chemical-looping technologies using circulating fluidized bed systems: Status of development, Fuel Process. Technol. 172 (2018) 1–12.

[15] D. Karami, A.H. Soleimanisalim, M.H. Sedghkerdar, N. Mahinpey, Preparation of Novel Oxygen Carriers Supported by Ti, Zr-Shelled γ-Alumina for Chemical Looping Combustion of methane, Ind. Eng. Chem. Res. 59 (2020) 3221–3228.
[16] H. Leion, Y. Larring, E. Bakken, R. Bredesen, T. Mattisson, A. Lyngfelt, Use of CaMn0.875Ti0.125O3 as oxygen carrier in chemical-looping with oxygen uncoupling, Energy Fuel 23 (2009) 5276–5283.
[17] I. Gogolev, C. Linderholm, D. Gall, M. Schmitz, T. Mattisson, J.B.C. Pettersson, A. Lyngfelt, Chemical-looping combustion in a 100 kW unit using a mixture of synthetic and natural oxygen carriers – Operational results and fate of biomass fuel alkali, Int. J. Greenhouse Gas Control 88 (2019) 371–382.
[18] M. Rydén, A. Lyngfelt, T. Mattisson, CaMn0.875Ti0.125O3 as oxygen carrier for chemical-looping combustion with oxygen uncoupling (CLOU)—experiments in a continuously operating fluidized-bed reactor system, Int. J. Greenhouse Gas Control 5 (2011) 356–366.
[19] M. Källén, M. Rydén, C. Dueso, T. Mattisson, A. Lyngfelt, CaMn0.9Mg0.1O3-δ as oxygen carrier in a gas-fired 10 kWth chemical-looping combustion unit, Ind. Eng. Chem. Res. 52 (2013) 6923–6932.
[20] C.A. Mims, J.K. Pabst, Alkali-catalyzed carbon gasification kinetics: unification of H2O, D2O, and CO2 reactivities, J. Catal. 107 (1987) 209–220.
[21] D. Gall, M. Pushp, K.O. Davidsson, J.B.C. Pettersson, Online measurements of alkali and heavy tar components in biomass gasification, Energy Fuel 31 (2017) 8152–8161.
[22] D. Gall, M. Pushp, A. Larsson, K. Davidsson, J.B.C. Pettersson, Online measurements of alkali metals during start-up and operation of an industrial-scale biomass gasification plant, Energy Fuel 32 (2018) 532–541.
[23] M. Öhman, A. Nordin, B.-J. Skrifvars, R. Backman, M. Hupa, Bed agglomeration characteristics during fluidized bed combustion of biomass fuels, Energy Fuel 14 (2000) 169–178.
[24] A.A. Khan, W. de Jong, P.J. Jansens, H. Spliethoff, Biomass combustion in fluidized bed boilers: potential problems and remedies, Fuel Process. Technol. 90 (2009) 21–50.
[25] I. Staničić, V. Andersson, M. Hanning, T. Mattisson, R. Backman, H. Leion, Combined manganese oxides as oxygen carriers for biomass combustion — ash interactions, Chem. Eng. Res. Des. 149 (2019) 104–120.
[26] I. Staničić, T. Mattisson, R. Backman, Y. Cao, M. Rydén, Oxygen carrier aided combustion (OCAC) of two waste fuels - Experimental and theoretical study of the interaction between ilmenite and zinc, copper and lead, Biomass Bioenergy 148 (2021), 106060.
[27] I. Gogolev, A.H. Soleimanisalim, C. Linderholm, A. Lyngfelt, Commissioning, performance benchmarking, and investigation of alkali emissions in a 10 kWth solid fuel chemical looping combustion pilot, Fuel 287 (2021), 119530.
[28] M. Pushp, D. Gall, K. Davidsson, M. Seemann, J.B.C. Pettersson, Influence of bed material, additives, and operational conditions on alkali metal and tar concentrations in fluidized bed gasification of biomass, Energy Fuel 32 (2018) 6797–6806.
[29] M. Schmitz, C.J. Linderholm, Performance of calcium manganate as oxygen carrier in chemical looping combustion of biochar in a 10kW pilot, Appl. Energy 169 (2016) 729–737.
[30] X.H. Li, F. He, F. Behrendt, Z.Q. Gao, J.R. Shi, C.Y. Li, Inhibition of K2SO4 on evaporation of KCl in combustion of herbaceous biomass, Fuel 289 (2021).
[31] V. Andersson, A.H. Soleimanisalim, X. Kong, F. Hildor, H. Leion, T. Mattisson, J.B. C. Pettersson, Alkali-wall interactions in a laboratory-scale reactor for chemical looping combustion studies, Fuel Process. Technol. 217 (2021), 106828.
[32] M. Zevenhoven, P. Yrjas, M. Hupa, Ash-Forming Matter and Ash-Related Problems, in, 2010.
[33] C. Sevonius, P. Yrjas, D. Lindberg, L. Hupa, Agglomeration tendency of a fluidized bed during addition of different phosphate compounds, Fuel 268 (2020), 117300.
[34] Z. Zhang, J. Liu, F. Shen, Z. Wang, Temporal release behavior of potassium during pyrolysis and gasification of sawdust particles, Renew. Energy 156 (2020) 98–106.
[35] P.H. Moud, K.J. Andersson, R. Lanza, J.B.C. Pettersson, K. Engvall, Effect of gas phase alkali species on tar reforming catalyst performance: initial characterization and method development, Fuel 154 (2015) 95–106.
[36] P. Instruments, Model 3062 diffusion dryer - instruction manual, in: TSI, 2003.
[37] H. WC, Aerosol Technology - Properties, Behavior and Measurement of Airborne Particles, Wiley, New York, 1999.
[38] K. Davidsson, K. Engvall, M. Hagström, J. Korsgren, B. Lönn, J. Pettersson, A surface ionization instrument for on-line measurements of alkali metal components in combustion: instrument description and applications, Energy Fuels 16 (2002).
[39] P. Hallberg, M. Hanning, M. Rydén, T. Mattisson, A. Lyngfelt, Investigation of a calcium manganite as oxygen carrier during 99h of operation of chemical-looping combustion in a 10kWth reactor unit, Int. J. Greenhouse Gas Control 53 (2016) 222–229.
[40] M. Rydén, H. Leion, T. Mattisson, A. Lyngfelt, Combined oxides as oxygen-carrier material for chemical-looping with oxygen uncoupling, Appl. Energy 113 (2014) 1924–1932.
[41] M. Pishahang, Y. Larring, M. McCann, R. Bredesen, Ca0.9Mn0.5Ti0.5O3−δ: a suitable oxygen carrier material for fixed-bed chemical looping combustion under syngas conditions, Ind. Eng. Chem. Res. 53 (2014) 10549–10556.
[42] P. Hallberg, M. Källén, D. Jing, F. Snijkers, J. van Noyen, M. Rydén, A. Lyngfelt, Experimental investigation of CaMnO3−δ based oxygen carriers used in continous chemical-looping combustion, Int. J. Chem. Eng. 2014 (2014), 412517.